ELSEVIER

Journal of Membrane Science 163 (1999) 29–38

journal of MEMBRANE SCIENCE

www.elsevier.nl/locate/memsci

# Heat and mass transfer in a membrane-based energy recovery ventilator

L.Z. Zhang*, Y. Jiang

*HVAC Division, Department of Thermal Engineering, Tsinghua University, Beijing, 100084, People's Republic of China*

Received 17 February 1999; received in revised form 19 April 1999; accepted 20 April 1999

**Abstract**

This paper presents a detailed heat and mass transfer model for an energy recovery ventilator (ERV) with a porous hydrophillic membrane core. Through finite difference simulations, the temperature, and humidity fields in the unit are calculated. The coupled heat and mass transfer mechanism for the system is discussed. It is found that for the present cross-flow arrangement, the membrane area is not effectively used in heat and moisture exchange. The heat and mass transfer rate is larger near the inlets of fluids. There is a ridge on the membrane in the direction of left-lower to upper-right where permeability is relatively higher. © 1999 Elsevier Science B.V. All rights reserved.

*Keywords:* Microporous and porous membranes; Gas and vapor permeation; Dehumidification; Thermodynamics; Air-conditioning

## 1. Introduction

Humidity control is a necessity for a variety of controlled spaces. The most widely practiced techniques of dehumidification include cooling coils, fixed adsorbent beds, absorption tower, and rotary wheel desiccant. These methods are bulky and very energy consuming since a large amount of energy is wasted in vapor phase change or desiccant regeneration [1]. The development in membrane science (especially pervaporation and gas separation) provides a new alternative to these traditional techniques. In recent years, membrane-based air dehumidification has drawn much attention since it offers a stable and continuous operable system that combines long life with low energy consumption [2].

Wang and Li [3] used synthesized zeolite membrane to remove water vapor from $H_2$ and $N_2$. Pan et al. [4] measured the permeability to water vapor of cellulose triacetate membranes of the asymmetric or skin type when they are in the form of hollow fibers. Wang et al. [5] studied the performance of a hollow fiber air drying module from the viewpoints of mass transfer coefficients and selectivity optimization. Cha et al. [6] used dried regenerated cellulose hollow fiber membranes to remove water vapor and VOCs from nitrogen. They found that the gel membrane system is the most efficient in vapor removing when the air is at high relative humidity levels.

These systems are very interesting and they continue to be actively pursued. However, they must be operated under very high pressure-difference and thus

*Corresponding author. Tel.: +86-10-62772072; fax: +86-10-62770544

*E-mail address:* lzzhang@te.tsinghua.edu.cn (L.Z. Zhang)


PII: S0376-7388(99)00150-7

high membrane intensity is required, which may be very problematic. Besides, the use of compressors (or vacuum pumps) also increases mechanical complexity and energy consumption.

Relatively little attention has been given to membrane-based energy recovery ventilator (ERV) – another application of water-permeable membrane in air-conditioning systems. ERV is an air-to-air heat exchanger where the two incoming streams (feed and sweep) have approximately the same pressure (near atmospheric), therefore the operation and maintenance of the system are very easy. The feed represents outdoor air (fresh air intake for a HVAC system). The sweep represents stale room air that would normally be exhausted through the ERV to the outside. If the core material of an ERV is vapor-permeable membrane, both heat and moisture are transferred between these two air streams when they flow through the unit. Thus heat and humidity would be recovered from the exhaust stream (sweep) in winter and excess heat and moisture would be transferred to the sweep in order to cool and dehumidify the incoming air (feed) in the summer. This application would increase the efficiency of the HVAC system since the latent heat load is responsible for a large fraction of the total load of air-conditioning.

In this paper, the mathematical model of the membrane-based ERV is setup. Through finite difference simulations, the performance and the heat and mass transfer mechanisms of the system are discussed. The temperature, humidity fields for both the feed and the sweep are obtained. The distribution of vapor osmosis rate is calculated.

## 2. Mathematical model

A schematic of a membrane-based ERV is shown in Fig. 1. The air-to-air heat exchanger incorporates a cubic core where the two air streams – the feed and the sweep flow in thin, parallel, alternating membrane layers in a cross-flow arrangement, in order to transfer heat and moisture from one air stream to the other. For the present study, both the temperature and the humidity at the inlet of the feed are higher than those at the inlet of the sweep. For reasons of symmetry, the calculation domain is selected as the three dimensional elementary cell represented in Fig. 2 by the

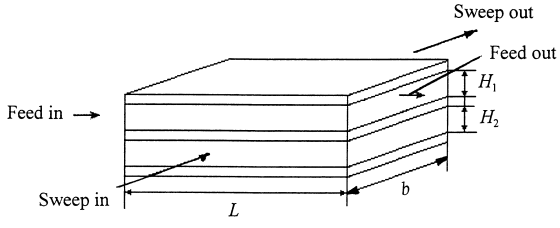


Fig. 1. Schematic of a cross-flow membrane-based ERV.

system boundary (dashed lines) and consists in half the volume distributed between two consecutive layers.

To aid in the model set up, several assumptions are made:

1. Heat and mass transfer processes are in steady state.
2. Heat conduction and vapor diffusion in the two air streams are negligible compared to energy transport and vapor convection by bulk flow.
3. Adsorption of vapor and membrane material is in equilibrium adsorption-state.
4. Both the heat conductivity and the water diffusivity in the membrane are constants.
5. Temperature and concentration distributions in the thickness direction in membrane are linear.
6. Water vapor diffusion in the membrane only occurs in the thickness direction.
7. Heat and moisture transfer in the air streams is two dimensional (in $x$ and $y$ directions), and heat transfer in membrane is three dimensional.

With the above assumptions, it is easy to deduce that the water osmosis rate in the membrane is a constant in the thickness direction. On the other hand, many studies of water-permeable membrane have already revealed that the selectivity of water/air is very high (in the range 460–30 000) [5], thus the air permeation through the membrane is neglected.

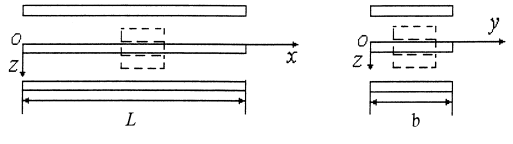


Fig. 2. Cross-section view of an elementary cell (surrounded by the dashed lines) in the ERV module.

The fundamental mass transfer of permeants from the feed side to the sweep side can be considered to occur in three steps [7], i.e.:

1. adsorption at the feed side of the membrane,
2. diffusion through the membrane,
3. desorption at the sweep side of the membrane.

### 2.1. Heat and mass conservation for the module

Feed:

$$\dot{m}_1 c_{p1} \frac{\partial T_{f1}}{\partial x} + \frac{2h_1}{H_1}(T_{f1} - T_{s1}) = 0, \tag{1}$$

$$\dot{m}_1 \frac{\partial \omega_1}{\partial x} + \frac{2k_1}{H_1}(\rho_{w1} - \rho_{s1}) = 0. \tag{2}$$

Sweep:

$$\dot{m}_2 c_{p2} \frac{\partial T_{f2}}{\partial y} + \frac{2h_2}{H_2}(T_{f2} - T_{s2}) = 0, \tag{3}$$

$$\dot{m}_2 \frac{\partial \omega_2}{\partial y} + \frac{2k_2}{H_2}(\rho_{w2} - \rho_{s2}) = 0. \tag{4}$$

Membrane:

$$\dot{m}_w c_{pw} \frac{\partial T_m}{\partial z} - \lambda_m \frac{\partial^2 T_m}{\partial x^2} - \lambda_m \frac{\partial^2 T_m}{\partial y^2} - \lambda_m \frac{\partial^2 T_m}{\partial z^2} = 0, \tag{5}$$

$$\dot{m}_w = -D_{wm} \frac{\partial C}{\partial z} = D_{wm} \frac{C_{1s} - C_{2s}}{\delta}, \tag{6}$$

where $C_{1s}$, $C_{2s}$ are water concentration in membrane at two surfaces (kg/m$^3$), $\delta$ is the membrane thickness.

The relation between $P_v$ and the total pressure of atmosphere $P$ is calculated by

$$P_v = \frac{\omega P}{\omega + 0.622}. \tag{7}$$

It is well known that surface diffusion and capillary condensation with liquid flow are the predominant mechanisms of water vapor and air separation by porous solid membrane [8]. The isotherms of water vapor and the porous membrane material used in this study can be expressed by the Dubinin and Radushkevich form (the D–R equation) [9]:

$$C = C_0 \exp\left\{-\gamma\left[T_m \ln\left(\frac{P_0}{P_v}\right)\right]^2\right\}, \tag{8}$$

where $C_0$ and $\gamma$ are coefficients which are obtained by adsorption experiments, $P_v$ is the water vapor partial pressure at the membrane surface, $T_m$ the membrane temperature, and $P_0$ is the corresponding saturated pressure of vapor at temperature $T_m$. This equation governs the relations between water concentration in membrane, vapor concentration in air and membrane temperature.

### 2.2. Boundary conditions

Feed:

$$T_{f1}|_{x=0} = T_{f1i}, \tag{9}$$

$$\omega_1|_{x=0} = \omega_{1i}. \tag{10}$$

Sweep:

$$T_{f2}|_{y=0} = T_{f2i}, \tag{11}$$

$$\omega_2|_{y=0} = \omega_{2i}. \tag{12}$$

Membrane:

$$\left.\frac{\partial T_m}{\partial x}\right|_{x=0} = 0, \tag{13}$$

$$\left.\frac{\partial T_m}{\partial x}\right|_{x=L} = 0, \tag{14}$$

$$\left.\frac{\partial T_m}{\partial y}\right|_{y=0} = 0, \tag{15}$$

$$\left.\frac{\partial T_m}{\partial y}\right|_{y=b} = 0. \tag{16}$$

Surface 1 of membrane (feed side):

$$-\lambda_m \left.\frac{\partial T_m}{\partial z}\right|_{z=0} = h_1(T_{f1} - T_m) + \dot{m}_w L_w. \tag{17}$$

Surface 2 of membrane (sweep side):

$$-\lambda_m \left.\frac{\partial T_m}{\partial z}\right|_{z=\delta} = -h_2(T_{f2} - T_m) + \dot{m}_w L_w \tag{18}$$

where $L_w$ is the latent heat of vaporization of water (kJ kg$^{-1}$).

### 2.3. Heat and mass transfer in boundary layers

#### 2.3.1. Calculation of heat transfer coefficients

Heat transfer in boundary layers is described by Nusselt correlations in which the Nusselt number, *Nu*

$$Nu = \frac{h d_e}{\lambda_f}$$

is related to the Reynolds number, *Re*

$$Re = \frac{u_f d_e}{\nu},$$

and the Prandtl number, *Pr*:

$$Pr = \frac{\mu c_{pf}}{\lambda_f},$$

where $d_e$ is the hydraulic diameter, and $L$ is the length of the flow channel. These parameters are often considered as a product, $\left(Re\,Pr\frac{d_e}{L}\right)$, which is helpful in obtaining the Nusselt number. Generally speaking, the Nusselt number increases with this product. However, the Nusselt number will asymptotically approach a lower limiting value as the product mentioned above is reduced. For pipe flow, this value is 3.658 for constant surface temperature and 4.364 for constant heat flux. For values of $Re\ Pr\ d_e/L$ less than approximately 100, Hausen's correlation is often recommended for the estimation of heat transfer coefficients for pipe flow in the laminar flow regime [10]

$$Nu = 3.658 + \frac{0.085(Re\,Pr(d_e/L))}{1 + 0.047(Re\,Pr(d_e/L))^{0.67}}\left(\frac{\mu_b}{\mu_s}\right)^{0.14}, \tag{19}$$

where subscript "b" refers to bulk, and "s" refers to surface. $\mu$ is the dynamic viscosity (kg/m s). For laminar pipe flow at higher values of $Re\ Pr\ d_e/L$, the Siedel–Tate correlation is often recommended [10]

$$Nu = 1.86\left(Re\,Pr\frac{d_e}{L}\right)^{0.33}\left(\frac{\mu_b}{\mu_s}\right)^{0.14}. \tag{20}$$

For turbulent pipe flow, the Dittus–Boelter correlation is recommended [10]

$$Nu = 0.023Re^{0.8}\,Pr^n, \tag{21}$$

in which $n$=0.4 if the fluid is being heated and $n$=0.3 if the fluid is being cooled.

For flow in rectangular channels, the same correlation as for pipe flow are recommended, provided that the correct hydraulic diameter is used. It should, however, be noted that the lower limiting value of the Nusselt number in the laminar flow regime is dependent on the geometry of the flow channel. In Fig. 3 this value is presented as a function of the aspect ratio, i.e. the relation between the height and the width of the channel, for two different assumptions regarding the heat transfer through the boundary layer [11].

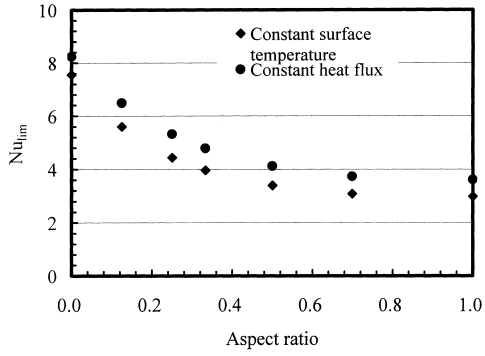


Fig. 3. The limiting Nusselt number for flow in rectangular channels with different aspect ratios, aspect ratio=channel height/channel width.

Hydraulic diameter for rectangular flow channel is

$$d_e = \frac{4bH}{2(b+H)}, \tag{22}$$

where $b$ is the width of the channel.

### 2.3.2. Calculation of mass transfer coefficients

Mass transfer in boundary layers is often described by Sherwood correlations in which the Sherwood number, *Sh*, is

$$Sh = \frac{kd_e}{D_{va}}, \tag{23}$$

where $D_{va}$ is the diffusivity of vapor in air ($m^2/s$). Convective mass transfer can be an analogy to convective heat transfer [11]. Then we have

$$Sh = Nu, \tag{24}$$

i.e.

$$k = \frac{h}{\rho_a c_{Pa} Le}, \tag{25}$$

where $\rho_a$ is the density of humid air; $c_{Pa}$ is the specific heat of humid air and *Le* is the Lewis number which is defined as

$$Le = \frac{\lambda_a}{\rho_a c_{Pa} D_{va}}. \tag{26}$$

### 2.4. Coefficients of performance

Sensible heat transferred through the ERV

$$Q = \dot{G}_1 c_{p1}(t_1 - t_3) = \dot{G}_2 c_{p2}(t_4 - t_2).$$

Sensible heat exchange power on the basis of unit membrane area

$$q = \frac{Q}{A}.$$

Total humidity transferred

$$D = \dot{G}_1(\omega_1 - \omega_3) = \dot{G}_2(\omega_4 - \omega_2).$$

The average permeability

$$Pe = \frac{D}{A}.$$

Total enthalpy transferred

$$I = \dot{G}_1(i_1 - i_3) = \dot{G}_2(i_4 - i_2),$$

where the specific enthalpy of the air can be calculated as

$$i = 1.005t + \omega(2501 + 1.86t).$$

Sensible effectivess

$$\mathrm{SE} = \frac{Q}{(\dot{G}c_p)_{\min}(t_1 - t_2)}.$$

Moisture effectivess

$$\mathrm{ME} = \frac{d}{(\dot{G})_{\min}(\omega_1 - \omega_2)}.$$

Enthalpy Effectivess

$$\mathrm{EE} = \frac{I}{(\dot{G})_{\min}(i_1 - i_2)}.$$

## 3. Results and discussion

### 3.1. Numerical methods and model validation

A prototype ERV is built and tested. The test facility is built around a currently marketed Carrier product – the so-called sensible heat recovery ventilator. The original paper core is replaced by UTC-MEM01, a novel porous hydrophilic polymer membrane prepared by UTRC. The temperature and the humidity are measured at the inlets and the outlets of two air streams. The experiments are conducted for two air-flow-rate cases: $\dot{G}_1 = \dot{G}_2 = \dot{G} = 0.01\,\mathrm{kg/s}$ and $\dot{G}_1 = \dot{G}_2 = \dot{G} = 0.05\,\mathrm{kg/s}$. The vapor permeability and the sensible heat exchange power can be obtained from these measured temperatures and humidities.

Before numerical analysis can be performed on the ERV system, the physical domain of the problem as well as the equations must be discretized. The whole calculating domain is divided into a number of equal-step discrete elements. Each element is identified as a control volume by a nodal point. The convection terms in the equations are approximated by the quadratic upstream differencing scheme (QUDS) [12] and the diffusion terms are replaced by the centered difference analogs. The nonlinearty of the equations is solved by iterative techniques. The three dimensional equations of the membrane are calculated by the means of ADI (alternating direction implicit) method [12]. It should be noted that since the membrane thickness is very small compared to the length and width, all variables must be in double-precision format to alleviate numeric error.

A computer program has been written to solve the problem. The dimensions of the ERV employed in the test and simulations are shown in Table 1.

The thermal diffusivity, $a$, of the membrane is measured to be $3.44\times10^{-6}\mathrm{m}^2/\mathrm{s}$. However, direct measurement of $D_{\mathrm{wm}}$, the effective diffusivity of water in the membrane, is difficult. In order to compare the theoretic and experimental results, a value for the $D_{\mathrm{wm}}$ has to be chosen for the use in the numerical model. The computer model is run for different values of $D_{\mathrm{wm}}$ using the experimental data. The ''true'' value chosen for $D_{\mathrm{wm}}$ is that, that makes the theoretical and experimental results agree well in the cases for one air-flow-

Table 1
Characteristics of the ERV studied

| Symbol | Value | Unit |
|---|---|---|
| $A$ | 4.645 | $\mathrm{m}^2$ |
| $L$ | 0.67 | m |
| $H_1$ | 0.01 | m |
| $H_2$ | 0.01 | m |
| $b$ | 0.24 | m |
| $\delta$ | 20 | μm |
| $C_0$ | 190.6 | $\mathrm{kg/m}^3$ |
| $\gamma$ | $1.80\times10^{-7}$ | $\mathrm{K}^{-2}$ |

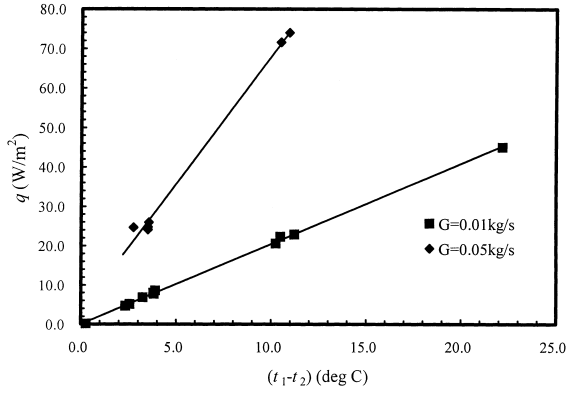


Fig. 4. The relations between sensible heat exchange power and temperature difference between two inlets, solid line: calculated; discrete dots: experimental.

Table 2
Parameters of the Feed and the Sweep

| Name | Symbol | Value | Unit |
|---|---|---|---|
| Feed in temperature | $t_1$ | 35.07 | °C |
| Feed out temperature | $t_3$ | 24.83 | °C |
| Sweep in temperature | $t_2$ | 35.07 | °C |
| Sweep out temperature | $t_4$ | 24.83 | °C |
| Feed in humidity | $\omega_1$ | 0.01966 | kg/kg |
| Feed out humidity | $\omega_3$ | 0.00306 | kg/kg |
| Sweep in humidity | $\omega_2$ | 0.00724 | kg/kg |
| Sweep out humidity | $\omega_4$ | 0.01538 | kg/kg |
| Feed flow rate | $\dot{G}_1$ | 0.01 | kg/s |
| Sweep flow rate | $\dot{G}_2$ | 0.01 | kg/s |

rate (0.01 kg/s). This value for $D_{wm}$ is $4.8\times10^{-10}$m$^2$/s. The calculated and experimental results for this flow-rate are shown in Figs. 4 and 5 in terms of sensible heat exchange power and permeability, respectively. To investigate how well do the experimental and theoretical results match in the cases other than those in which they are forced to match, the experimental and theoretical results for the other air-flow-rate (0.05 kg/s) are also plotted in Figs. 4 and 5. As can be seen, the agreement of the results calculated and experimentally obtained is generally good. It suggests that the model can be used to study the heat and mass transfer mechanisms in the membrane-based ERV.

### 3.2. Heat and mass transfer in the module

Using the model, the temperature and the humidity are calculated for both the feed and the sweep for one case study. The parameters of the fluids at inlets (pre-set) and at outlets (calculated) are shown in Table 2.

In Figs. 6 and 7 are shown the contours of the temperature distribution in the feed and in the sweep, respectively. The feed flows in $x$ direction, and the sweep flows in $y$ direction. The isotherms in the air streams are parallel to the diagonal line (left-lower to upper-right). The thermal gradients are much higher in

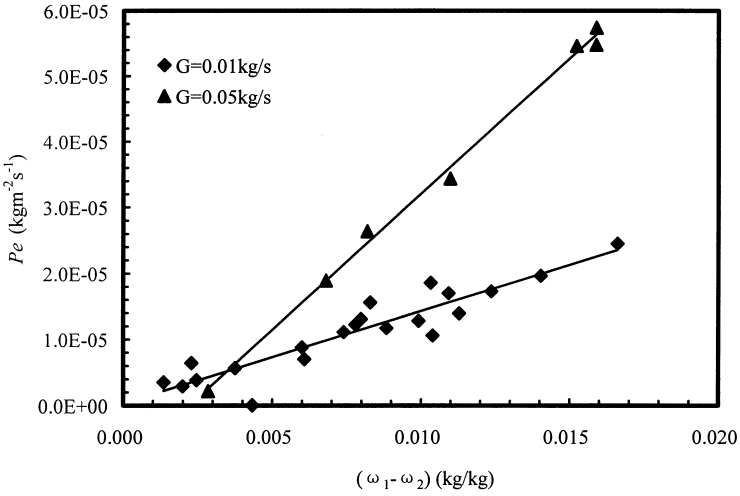


Fig. 5. The relations between permeability and humidity difference of two inlets, the solid line: calculated; the discrete dots: experimental.

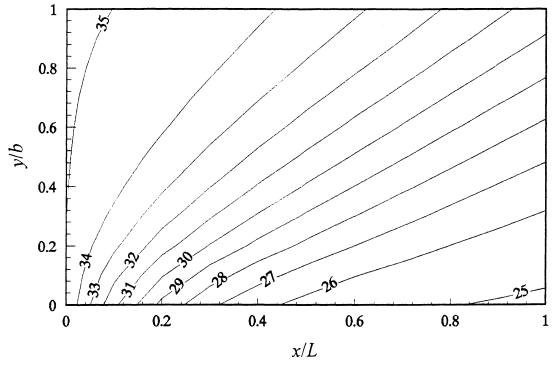


Fig. 6. The contour of temperature of the feed (°C).

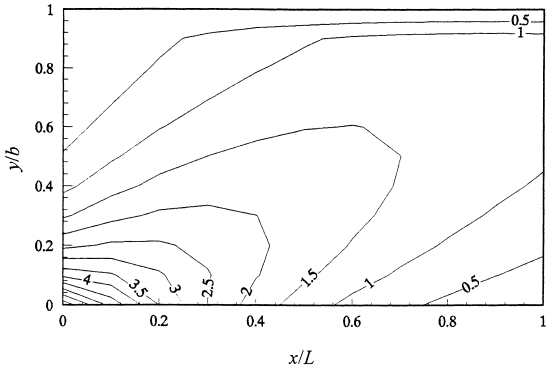


Fig. 8. The contour of the temperature difference between the feed and the sweep (°C).

the diagonal region than those in the left-upper and right-lower regions. The temperature difference between the two fluids is shown in Fig. 8. As can be seen, a relatively big temperature difference can only be maintained across a small portion of membrane area near the inlets. The membrane area is not effectively used in sensible heat exchange. This problem can be overcome by counter-flow arrangement.

In Figs. 9 and 10 are shown the contours of the humidity distribution in the feed and in the sweep, respectively. The shapes of the humidity contours are similar to those of the temperature. The humidity contours in the air streams are also parallel to the diagonal line (left-lower to upper-right). This in another side discloses the analogy between heat transfer and mass transfer. The humidity gradients are much higher in the diagonal region than those in the left-upper and right-lower regions. The humidity

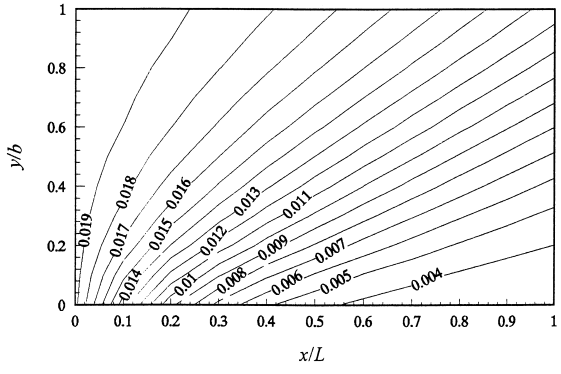


Fig. 9. The contour of the humidity of the feed (kg/kg).

difference between the two fluids is shown in Fig. 11. As can be seen, a relatively big humidity difference can only be maintained across a small portion of membrane area near the inlets. The membrane area

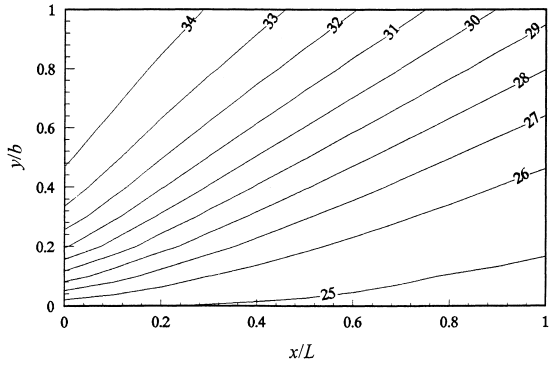


Fig. 7. The contour of temperature of the sweep (°C).

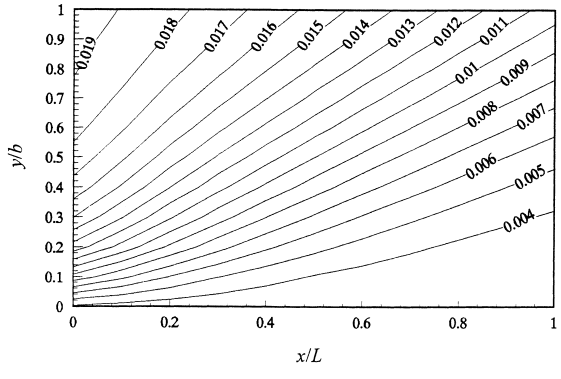


Fig. 10. The contour of the humidity of the sweep (kg/kg).

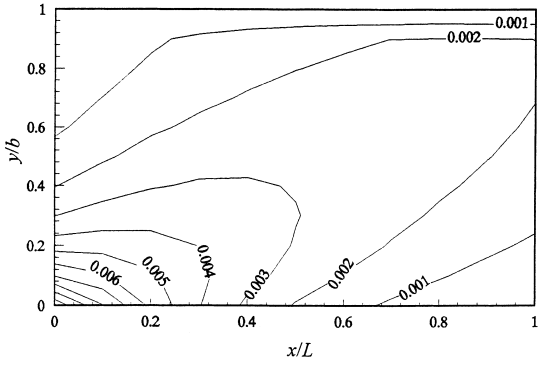


Fig. 11. The contour of the humidity difference between the feed and the sweep (kg/kg).

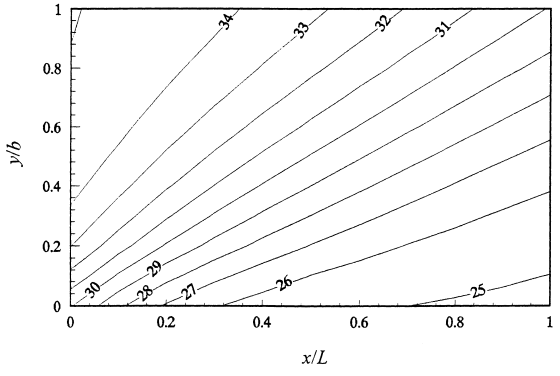


Fig. 12. The contour of the temperature of the membrane (°C).

is not effectively used in moisture exchange. This problem can also be overcome by counter-flow arrangement. In Table 3, performance comparison is made among ERVs with different cores and flow arrangements. As can be seen, the sensible only ERV has the highest sensible effectivess, but has the lowest enthalpy effectivess. The membrane-based ERV with counter flow arrangement performs the best. Energy saving analysis has been made using a software named DeST. The computed results shown that 18.0% and 23.5% of total energy consumed in a traditional HVAC system during a whole year can be saved by a Sensible Only ERV and a membrane-based cross-flow ERV, respectively, for a commercial building in Beijing.

### 3.3. Heat and mass transfer in the membrane

Ever though the thickness is very small compared to the length and the width for the membrane, the heat transfer in the membrane is in three dimension due to very small temperature difference in thickness direction (the difference in other two directions are relatively larger). A cross-section view of the temperature distribution in the membrane is shown in Fig. 12. On the other hand, numerical results reveal that the temperature difference between the two surfaces of membrane is in the order of $10^{-4}$°C resulted from very small thickness, so the temperature difference in thickness can be neglected. The shapes of the isotherms in the membrane are similar to those in the feed and sweep. The value of the membrane temperature is the half of the feed temperature and sweep temperature combined at the same location.

The driving force for water vapor transfer is mainly the humidity difference of two fluids. The distribution of the contours of humidity difference (Fig. 11) affects the vapor osmosis rate through the membrane. Fig. 13 shows the contour of permeability across the membrane. The permeability is very high near the inlets of two fluids. But it decreases rapidly with an increase in

Table 3
Performance comparisons of different types of ERV

| Types of ERV | SE | ME | EE |
|---|---|---|---|
| Sensible only ERV | 0.762 | 0 | 0.154 |
| ERV with paper core | 0.691 | 0.362 | 0.433 |
| ERV with membrane core (cross) | 0.752 | 0.748 | 0.743 |
| ERV with membrane core (counter) | 0.821 | 0.816 | 0.818 |

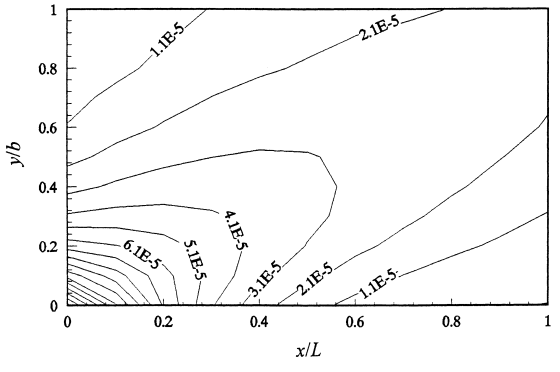


Fig. 13. Contour of the vapor permeability across the membrane (kg $m^{-2}$ $s^{-1}$).

membrane length and/or width. When the $x/L$ and/or $y/b$ is bigger than 0.5, the step of decrease tends to be very small with a further increase in coordinates. This figure indicates that there is a ridge in the direction of left-lower to upper-right where permeability is relatively high. The average permeability for the entire membrane is $2.5\times10^{-5}$ kg/m$^2$ s.

## 4. Conclusions

The application of membrane-based ERV is a new area of membrane-based dehumidification. Both heat and moisture are transferred between the two air streams when they flow through the unit. Heat and humidity would be recovered from the exhaust stream (sweep) in winter and excess heat and moisture would be transferred to the sweep in order to cool and dehumidify the incoming air (feed) in the summer. The efficiency of the HVAC system can be improved.

This paper presents a detailed heat and mass transfer model for an ERV with a porous hydrophilic membrane core. The coupled heat and mass transfer mechanisms for the system are discussed. It is found that for the present cross-flow arrangement, the membrane area is not effectively used either for sensible heat or for moisture transfer. With counter flow arrangement, the sensible effectivess, the moisture effectivess, and the enthalpy effectivess can be even higher. The temperature difference between two surfaces of the membrane can be neglected. The distribution of the contours of humidity difference affects the vapor osmosis rate through the membrane. The permeability is very high near the inlets of two fluids but relatively lower at other sites. This suggests that there is a ridge in the direction of left-lower to upper-right where permeability is relatively higher. The average permeability for the entire membrane is $2.5\times10^{-5}$ kg/m$^2$ s under present operating conditions. The effectivess of sensible heat exchange, moisture exchange, and the enthalpy exchange is promising.

## 5. Nomenclature

| | |
|---|---|
| $a$ | thermal diffusivity (m$^2$/s) |
| $A$ | membrane area (m$^2$) |
| $b$ | width of the flow channel (m) |
| $c_p$ | specific heat (kJ/kg K) |
| $C$ | water concentration in membrane (kg/m$^3$) |
| $d_e$ | hydraulic diameter (m) |
| $D$ | moisture transfer rate (kg/s) |
| $D_{va}$ | diffusivity of vapor in air (m$^2$/ s) |
| $D_{wm}$ | diffusivity of water in membrane (m$^2$/s) |
| $\dot{G}$ | total mass flow rate of air streams (kg/s) |
| $h$ | convective heat transfer coefficient (kW/ m$^2$ K) |
| $H$ | height of the flow channel (m) |
| $k$ | convective mass transfer coefficient (m/s) |
| $L$ | length of the flow channel (m) |
| $L_w$ | latent heat of vaporization of water (kJ/kg) |
| $\dot{m}$ | mass flow-rate for unit cross-section area (kg/m$^2$ s) |
| $P$ | pressure (Pa) |
| $Q$ | heat transfer rate (kW) |
| $R$ | ideal gas constant (J/kg K) |
| $T$ | temparature (K) |
| $x$, $y$, $z$ | coordinates (m) |
| $\gamma$ | coefficient in adsorption isotherms of membrane-vapor (K$^{-2}$) |
| $\lambda$ | thermal conductivity (kW/m K) |
| $\delta$ | thickness of membrane (m) |
| $\omega$ | humidity (kg water/kg air) |
| $\mu$ | dynamic viscosity (Pa s) |
| $\rho$ | density (kg/m$^3$) |

*Subscripts*

| | |
|---|---|
| a | air |
| f | fluids |
| i | inlet |
| m | membrane |
| s | Surface |
| v | vapor |
| w | water |
| 1 | feed, feed inlet |
| 2 | sweep, sweep inlet |
| 3 | feed outlet |
| 4 | sweep outlet |

## Acknowledgements

The authors are grateful for the financial and technical support from UTRC of USA.

## References

[1] G.W. Brundrett, Handbook of Dehumidification Technology, Butterworths, London, 1987.
[2] U. Sander, H. Janssen, Industrial application of vapour permeation, J. Membr. Sci. 61 (1991) 113–129.
[3] J.Q. Wang, Z. Li, Synthesis of zeolite membrane and its application in removal of moisture from gases, Membr. Sci. Tech. (in Chinese) 18 (1998) 54–58.
[4] C.Y. Pan, C.D. Jensen, C. Bielech, H.W. Habgood, Permeation of water vapor through cellulose triacetate membranes in hollow fiber form, J. Appl. Polym. Sci. 22 (1978) 2307–2323.
[5] K.L. Wang, S.H. Mccray, D.D. Newbold, E.L. Cusseler, Hollow fiber air drying, J. Membr. Sci. 72 (1992) 231–244.
[6] J.S. Cha, R. Li, K.K. Sirkar, Removal of water vapor and VOCs from nitrogen in a hydrophilic hollow fiber gel membrane permeator, J. Membr. Sci. 119 (1996) 139–153.
[7] S.H. Chen, R.C. Ruaan, J.Y. Lai, Sorption and transport mechanism of gases in polycarbonate membranes, J. Membr. Sci. 134 (1997) 143–150.
[8] M. Asaeda, L.D. Du, Separation of alcohol/water gaseous mixtures by thin ceramic membrane, J. Chem. Eng. Jpn. 19 (1986) 72–77.
[9] M. Suzuki, Adsorption Engineering, Kodansha, Tokyo, 1989.
[10] H.O.E. Karlsson, T. Gun, Heat transfer in pervaporation, J. Membr. Sci. 119 (1996) 295–306.
[11] F.P. Incropera, D.P. Dewitt, Fundamentals of heat and mass transfer, 3rd ed., Wiley, New York, 1990.
[12] R. Peyret, T.D. Taylor, Computational Methods for Fluid Flow, Springer, New York, 1990.